AAS 88-005

TWENTY MILLIARCSEC POINTING SYSTEM FOR THE ROLLING GP-B SPACECRAFT

Bradford W. Parkinson* **and N. Jeremy Kasdin†**

The Stanford Relativity Gyro Experiment (GP-B) is a space based experiment to verify two previously untested predictions of Einstein's theory of General Relativity. These predictions are that a local inertial frame in Earth orbit will drift with respect to the universe's inertial (non-rotating) frame. Frame motion is measured by a near perfect gyroscope in a 650 km polar orbit by determining its spin axis motion with respect to the chosen guide star (Rigel) with an accuracy better than 1 milliarcsecond. The attitude sensor is a special quartz telescope maintained at cryogenic temperatures. The actuators are continuously firing, proportional thrusters which have been developed at Stanford. The pointing control system keeps the telescope axis aligned with the line of sight to the star to within 20 milliarcsec rms. Simulations verify this pointing accuracy.

INTRODUCTION

The Stanford Relativity Gyroscope Experiment (NASA's Gravity Probe B) was conceived in 1960 by L.I. Schiff, then Chairman of the Department of Physics at Stanford University, as a space-based test of Einstein's General Theory of Relativity. The basic idea for GP-B is deceptively simple: to measure the spin axis drift of an Earth orbiting gyroscope relative to inertial space with an accuracy of 1 milliarcsec/year. The difficulty arises in building gyros and a measurement system with this required accuracy. The past twenty-five years have been marked by continued development of the necessary technologies at Stanford, the Marshall Space Flight Center, and more recently at Lockheed's Palo Alto Research Laboratories, with the present schedule targeting launch for 1994.

* Dr. Parkinson is a Research Professor in the Aeronautics and Astronautics Department and High Energy Physics Laboratory of Stanford University and the Program Manager of the Stanford Relativity Gyro Experiment, Stanford, California 94305.

† Mr. Kasdin is a Ph.D. student in the Aeronautics and Astronautics Department at Stanford University, Stanford, California 94305.

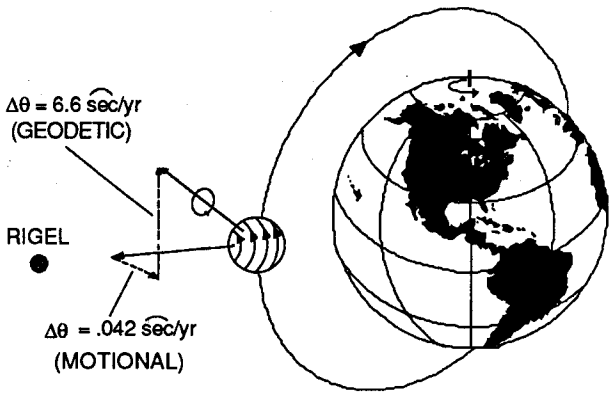

Figure 1: Relativistic Effects on Gyroscope[4]

Einstein's theory predicts two orthogonal effects for a gyro in a 650 km circular, polar orbit that do not appear in Newtonian gravitation; these are depicted schematically in Fig. 1. The geodetic drift is the larger of the two, accounting for a 6.6 arcsec/yr drift in the plane of the orbit. This rotation of the gyro's locally-inertial frame is due to its motion within the gravity field of the Earth. The second, and perhaps more interesting, effect is the frame dragging drift. Though significantly smaller (only 42 milliarcsec/yr), this prediction is important because it is analogous to the magnetic field, bringing the gravitational theory closer to a unification with electromagnetism. Just as a magnetic field results from the motion of charged particles, the frame dragging effect is caused by a dragging of the gyro's locally inertial frame by the massive Earth's rotation. For this reason it is often called the gravitomagnetic effect.[1,2,3,4]

For the control engineer, one challenge of this experiment is maintaining an inertial reference from which to measure the gyro's spin axis motion. This inertial reference is obtained by pointing the satellite via a star tracking telescope at an inertially calibrated guide star, Rigel.† Relativity information is then determined by differencing the gyro and telescope signals. Rigel is the seventh brightest star in the sky and located approximately 8 degrees below the celestial equator and 500 light years from Earth. One fringe benefit of the experiment will be to improve our measurement of the distance to Rigel, and thus the distance scale of the universe, by 30 percent.

The GP-B satellite and its attitude control system are unique in both the precision required and in the new and innovative hardware being used. Never before has a rolling satellite been flown with an inertial stability requirement of better than 70 milliarcseconds. This pointing accuracy will be met by using a star-splitting telescope as a two-axis star tracker. Proportional thrusters, operating continuously, will be used for control. Finally, this precise control must be accomplished with a small maximum thrust (less than 70 dynes per thruster) and with minimal angular accelerations.

---

† *It is recognized that stars are not fixed but can have significant proper motion. It is anticipated, however, that Hipparcos, the European astronomy satellite, will calibrate the proper motion of Rigel to the required accuracy.*

The current GP-B control system is a demonstration of the interdependence of the spacecraft subsystems. Thus, as the various subsystems continue to evolve, so will the attitude control system. For example, the solar cell design was recently changed from a panel configuration to a ring, reducing drag and creating roll symmetry. This change, however, affected the mass and stiffness properties of the satellite and required modification of the control system. By developing a design methodology with attendant software we are creating the tools necessary for easy evolution of the control system and verification of the mission requirements as the spacecraft design approaches its final form.

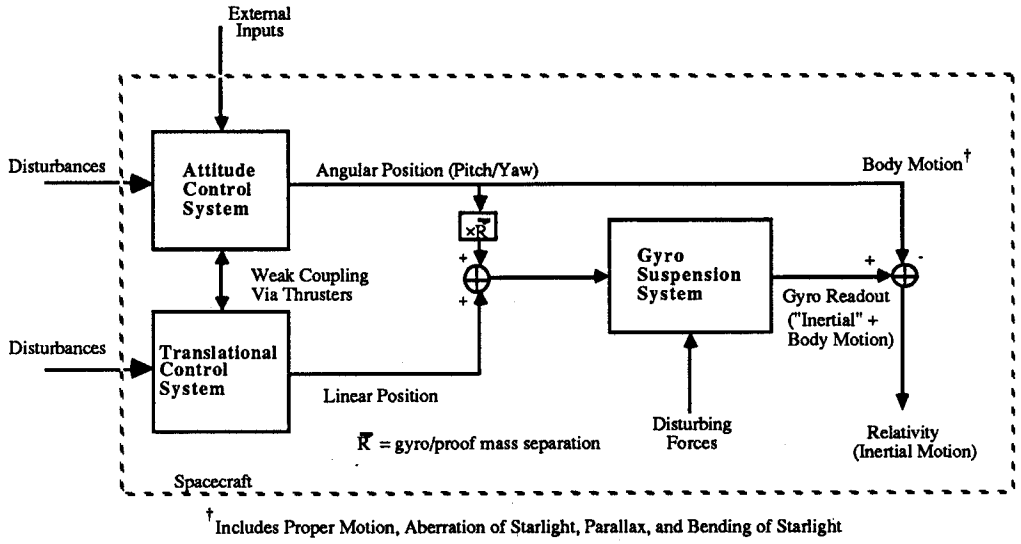

Figure 2: GP-B Integrated Control System

Fig. 2 is a schematic of the overall GP-B integrated control system. This paper presents the progress to date in designing the attitude control. It discusses the requirements on the pointing control system and the disturbances acting upon the spacecraft. It also presents candidate control system designs and simulations to verify the feasibility of the mission. The translational drag free control system has been discussed elsewhere.[1,2,5,6,7] It was used on the Navy's Transit Navigation Satellite Triad I in 1968 achieving accelerations as low as 5×10^{-12}g. Its influence on the attitude control system will be discussed below. The gyro suspension system has also been independently designed and tested.[6,8] This paper will present how this system influences the requirements on attitude control.

The next section describes the satellite and the associated hardware being developed for the GP-B mission. Emphasis is placed on the star-tracking telescope and the proportional thrusters and how they impose limitations on the pointing control system. Following this is a brief summary of additional issues which will be covered in future simulations. The next section presents the specifications of the control system necessary to achieve the desired 1 marcsec/yr accuracy. Finally, classical and modern control system designs are presented with simulation results that indicate the basic mission requirements can be met.

SATELLITE HARDWARE

Spacecraft

The GP-B satellite (Fig. 3) is about 4.3 m long and wide and weighs about 1500 kg[5]. It will roll with a 10 minute period about its axis of symmetry, which points at the guide star. Roll was introduced to help alleviate a number of problems, including averaging out of many of the Newtonian torques on the gyros, elimination of problems of null drift in the telescope and gyro readout systems, and reduction of the effect of gyro readout noise (1/f) by moving the drift information in body axes to a higher frequency[4]. The roll period was kept low, however, to minimize the effect of centrifugal accelerations on the rotors.

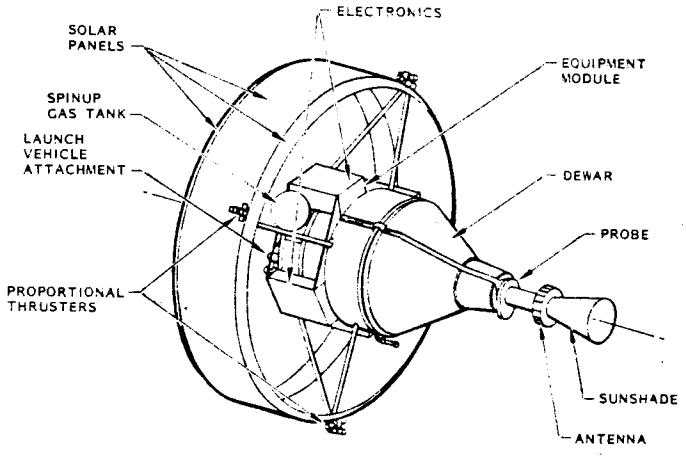

Figure 3: GP-B Satellite Concept[5]

The GP-B experiment module is depicted in Fig. 4. The principal elements of the experiment, the gyros and their housings, are contained in a quartz block assembly that is optically contacted to the quartz telescope. The quartz block is then attached via a support cylinder to the vacuum probe. This entire assembly is surrounded by a layering of magnetic shielding, including a supercooled lead bag and a mu-metal shield, reducing the ambient field at the gyroscope to 10^{-7} gauss.[4,9] This in turn is surrounded by a tank of superfluid helium that keeps the experiment at a constant temperature of 1.7 °K. All of the reasons for supercooling the experiment are beyond the scope of this paper, but one benefit of maintaining the telescope and quartz block assembly at this low temperature is a reduction in errors due to thermal expansion and creep.

The helium tank or dewar is attached to the outer structure of the satellite by 12 passive orbital disconnect struts (PODS-IV), depicted in Fig. 5. These devices provide a very high stiffness to thermal conductivity ratio and their importance to disturbance rejection and control system design will be discussed below.[5,10]

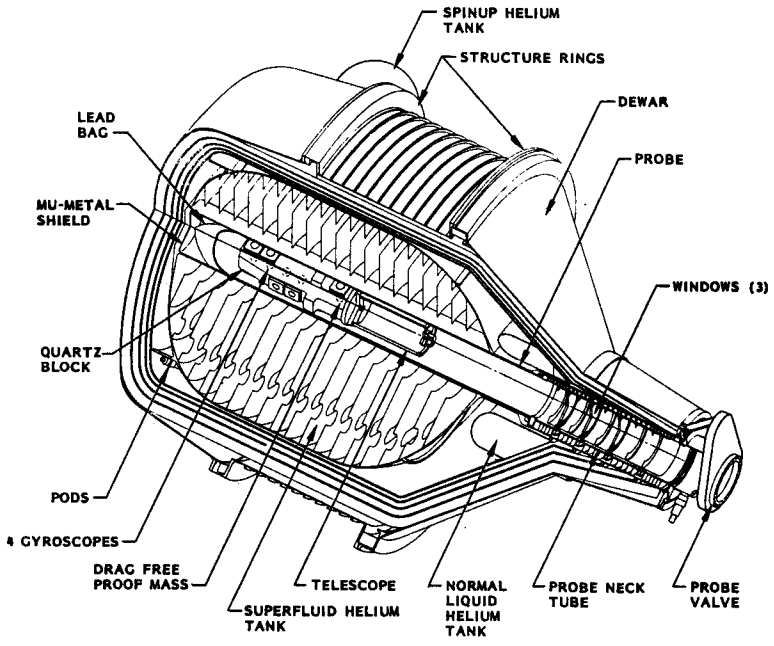

Figure 4: GP-B Experiment Module[4]

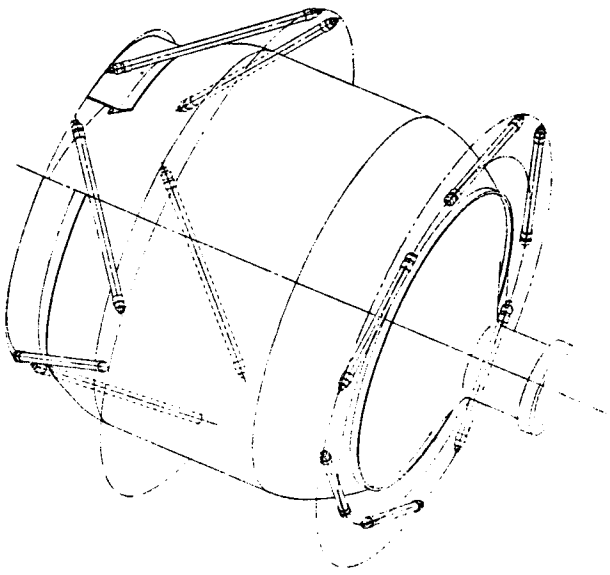

Figure 5: PODS-IV Supports[10]

Telescope

The telescope (Fig. 6) is a Schmidt-Cassegranian type with a 150 in. focal length, 5.6 in aperture, and 14 in. overall length. It provides attitude by splitting the stellar light beam into two opposing beams in each of two orthogonal directions. Each pair of beams is collected and attitude is inferred by comparing the amount of light at each photomultiplier.

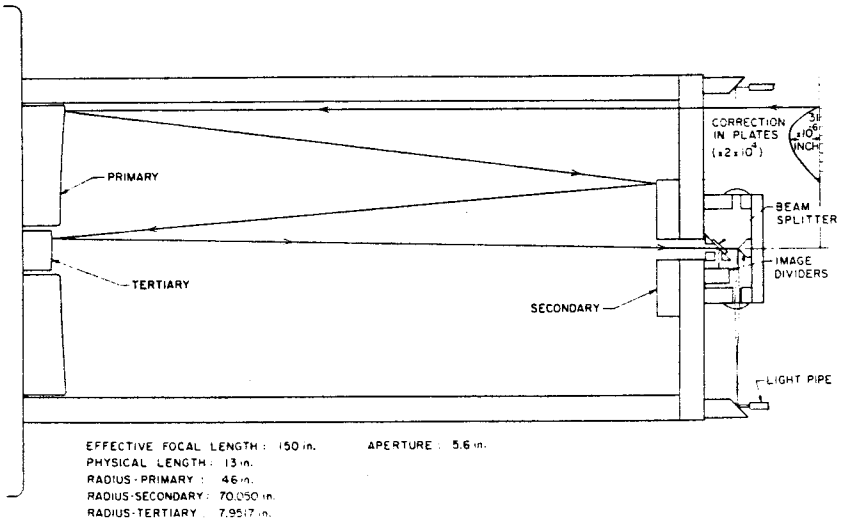

Figure 6: Optical Layout of Cryogenic Telescope[11]

The telescope is expected to have a precision of 0.1 marcsec over its linear range of 70 marcsec (which defines the pointing accuracy requirement on the attitude control system). The current requirement places telescope noise at 3 marcsec in a 10 Hz bandwidth[11]. This low noise is important both for the performance of the attitude control system and for achieving the 1 marcsec precision of the experiment. Everitt[11] details how this low noise level is achieved. By operating in space, the limitations on Earth based telescopes of atmospheric turbulence and distortion and creep due to the weight of the structure are removed. Operating at cryogenic temperatures eliminates distortion due to temperature gradients. Through proper choice of photodetector, the electronics' noise can be reduced to negligible levels. The noise performance is then determined by the "photon limit", that is, fluctuations caused by random arrivals of photons. Everitt calculates this to be, for Rigel as the guide star, about 1 marcsec in a 1 second observation time.

The telescope will also have a null stability of better than 0.1 marcsec over the 10 minute roll period, but may have a 20% scale factor change over the life of the experiment. A prototype of the telescope has been constructed and tested at Stanford.

Thrusters

The attitude and translational actuators for the GP-B spacecraft are continuously operating proportional thrusters fueled by the boiloff superfluid helium gas. The primary motivation for choosing this unconventional type of actuator was in solving the boiloff helium problem. If some other type of actuation was used, the helium gas venting to space would prove to be the largest disturbance affecting the spacecraft. Conventional on-off thrusters were ruled out because of reliability concerns; the high pointing accuracy of the GP-B experiment would require upwards of 10^7 firings over the one year experiment. Also, this stringent accuracy would require such a small deadband and hysteresis cycle that the high accelerations during firing could result in an unacceptable gyro environment.

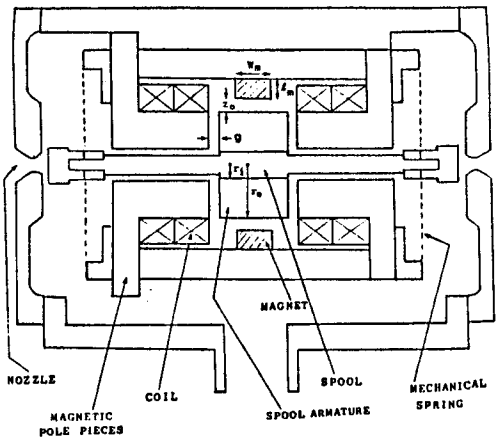

Figure 7: The Differential Thruster Design[13]

As a result, Stanford developed the low thrust, continuous, differential thruster depicted in Fig. 7.[12,13] Nominally, the spool is centered, allowing equal flow through each nozzle (at a Reynold's number of about 36). To obtain differential thrust, the spool is moved by a solenoid in either direction, constricting flow in that direction and allowing more flow through the opposing nozzle. Because of limitations in the spool/solenoid arrangement the open loop bandwidth of the thruster is limited to 100 Hz. This 100 Hz bandwidth is sufficient to satisfy the low bandwidth requirements of the satellite control system.[13]

Much effort has been expended on improving the linearity of the thrusters. The present design has less than 6% hysteresis due to the ferromagnetic spool. The thruster is linear within its operating range to better than 5%. There are twelve thrusters symmetrically spaced about the spacecraft, providing 4 thrusters per axis. For conservatism, this analysis assumes a maximum capability equal to one-half of the available thrust.. A calculation is made below of the expected drag force on the satellite. The result is that 90 dynes of thrust are needed for the drag free control system to compensate for drag. Since each thruster has a maximum thrust of 70 dynes, there is 50 dynes per axis available for attitude control. Allowing for a two meter moment arm, 10,000 dyne-cm of torque is available for pointing. The present nominal design parameters are summarized in Table 1.

Table 1

Nominal Thruster Design Parameters

Mass Flow Rate:	5.5×10^{-4} gm/sec
I_{sp}:	130 sec
Maximum Thrust:	70 dynes/thruster
Maximum Torque:	10,000 dyne-cm
R.M.S. Noise:	50 dyne-cm/thruster

ADDITIONAL REQUIREMENTS AND CONSTRAINTS

This control design will accommodate all of the major requirements and constraints. However, we expect further refinements as the full spacecraft design matures. This paper's purpose is to introduce the requirements and problems associated with the GP-B spacecraft and show the viability of steady state control under the assumed spacecraft model. Transients and initial star acquisition of the guide star will be completed soon. Also, the issue of controlling the spacecraft while the Earth blocks the star from the telescope's view is the subject of a separate effort to be reported on later. For this occulted operation, the gyros will be used as attitude sensors. Once a final design is completed for the telescope phase, it can be modified for use during occultation.

The roll control system has been discussed elsewhere and is well established.[6,12] It will use a rate gyro and a star blipper for roll phase updates and is anticipated to perform within specifications. The problem of helium slosh as a disturbance has not been investigated in detail, but preliminary analyses[10,15] show that the baffles used in the tank reduce this torque to levels well below those of the other disturbances.

Lorell[14] developed an active inertia trimming technique using moving masses about two axes. It is likely that such a technique will be used to bring the principal axes of inertia to within half a degree of the geometric axes. However, this is a slow process and will only be done periodically, so it does not directly impact the pointing control design.

It has been demonstrated that the mu-metal shield when exposed to the magnetic field of the Earth has an induced magnetization of 100,000 gauss-cm. Because the shield is cylindrical, this moment is not aligned with the ambient field and results in a maximum torque of 20,000 dyne-cm.[15,16] Preliminary calculations suggest that magnetic torquers can effectively cancel this slowly changing disturbance.

Finally, this is a time-invariant, linear analysis. Because of the fine pointing requirements, a linear spacecraft model is an excellent one for design purposes. However, there are various non-linear effects in the thrusters and telescope that will be included in the final simulation. These include hysteresis, bias, small non-linearities in response, saturation of the thrusters, and scale factor drift.

MISSION REQUIREMENTS

Pointing Accuracy

As stated above, the requirement on the attitude control system is 20 marcsec rms per axis with a 70 marcsec maximum deviation. The control system has to achieve this accuracy in the presence of disturbances, with limited available thrust, and within the acceleration constraints discussed below.

Because the telescope is an error sensor rather than an inertial attitude sensor, the spacecraft will slew to keep the star image centered. This image appears to move (apart from the stars proper motion) due to four optical effects. The largest of these effects is stellar aberration caused by satellite motion perpendicular to the line of sight to the star. Annual aberration is ±20.49 arcsec with a one year period and results from the Earth's motion about the Sun

while orbital aberration is ±5 arcsec and results from the satellite orbiting the Earth. The other two effects are relativistic bending of starlight by the Sun, ±0.0144 arcsec, and stellar parallax, ±0.007 arcsec. All of these occur at very low frequency and require less than 0.5 dyne-cm, thus having negligible impact on the pointing control system.

Attitude Acceleration Limits

In addition to the usual requirements, the rotors' electrostatic suspension system places an additional limit on the acceleration of the satellite. To reduce acceleration induced torques on the rotors it is important that attitude motion about the center-of-mass not create excessive forces on the gyros. Keiser[12] determined the limits on housing acceleration that would cause unacceptable drift of the gyros due to the suspension system acting upon their slight out-of-roundness. He found that the rms rotor acceleration must be less than 2×10^{-7}g, or 200 nanog, and that accelerations at roll frequency must be less than 1×10^{-10}g. For a 45 cm gyro to center-of-mass spacing, this corresponds to a angular accelerations of 900 marcsec/sec^2 and 0.45 marcsec/sec^2 respectively.

CONTROL SYSTEM DESIGN

System Model

Fig. 8 shows the present attitude control system concept in rolling body axes referred to in Fig. 2. As discussed below, the bandwidth of the pointing control system for each axis is about 0.25 Hz, 150 times the roll frequency. Because we are rolling so slowly, the gyroscopic coupling cannot be used for control and appears merely as a small, low frequency disturbance. For design, each axis is considered separately. The roll coupling is included in the simulation, however. For the simulations here, the spacecraft is assumed to be rolling at a constant rate.

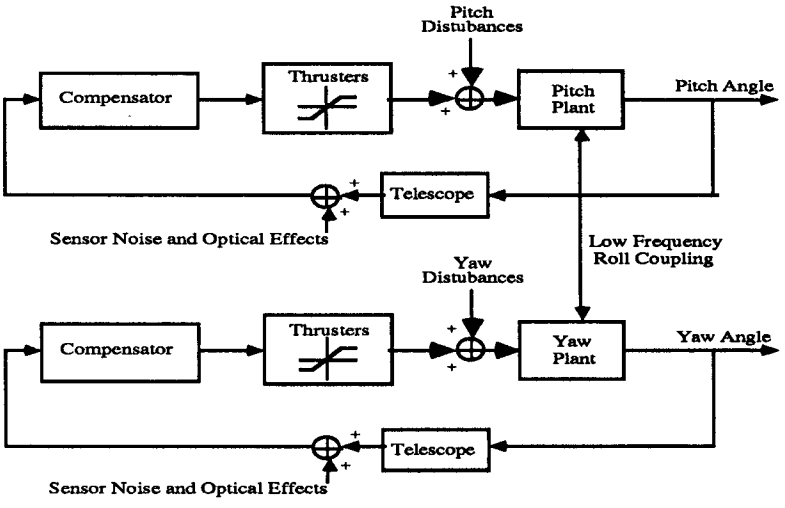

Figure 8: Attitude Control System

Dynamic Model

Fig. 9 shows the dynamic model being used for the spacecraft. The elastic connection results from the PODS-IV support of the helium tank and vacuum probe and is expected to have a 30 Hz resonance. The equations of motion for this system are found by determining Euler's equations for motion of each body expressed in its body axes and then introducing a spring torque proportional to the relative angular displacement of each body about the pitch and yaw axes.

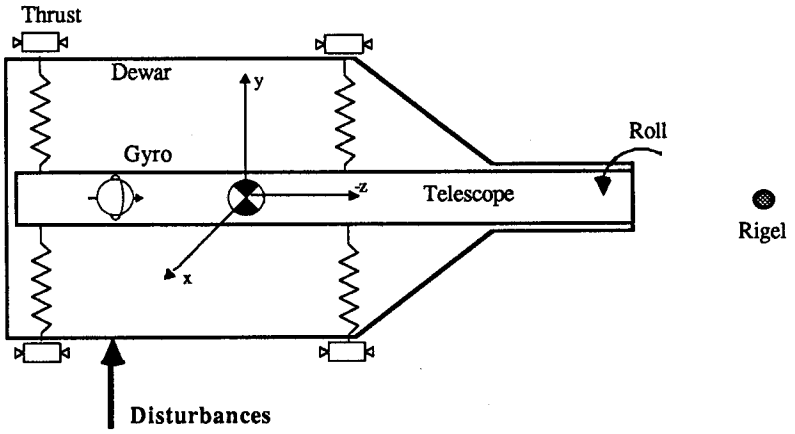

Figure 9: Spacecraft Dynamic Model

Euler's equations were determined using a method developed by Parkinson[18] that easily accounts for small products of inertia caused by a principal axis misalignment. The inertia dyadic is written in matrix form as:

$$\mathbf{I} = I_z \begin{bmatrix} 1-\varepsilon_1 & 0 & \varepsilon_3 \\ 0 & 1-\varepsilon_2 & \varepsilon_4 \\ \varepsilon_3 & \varepsilon_4 & 1 \end{bmatrix} \tag{1}$$

Where I_z is the principal inertia about the roll axis (note that here boldface indicates vector quantities expressed in the satellite body axes). The GP-B spacecraft is a major axis spinning, symmetric satellite, so $\varepsilon_1 = \varepsilon_2 > 0$. Determination of the product of inertia terms will be discussed below. The angular velocity vector of the body with respect to inertial space is written as:

$$\mathbf{W}_{b/i} = \begin{bmatrix} W_x \\ W_y \\ \beta \end{bmatrix} \tag{2}$$

Where W_x and W_y are small pitch and yaw angular velocities and β is the constant roll rate. The vector form of Euler's equations (written in body axes) is:

$$\overset{b}{\mathbf{W}}_{b/i} = \mathrm{I}^{-1}\left\{ -\left[\mathbf{W}_{b/i}\times\right]\mathbf{I}\cdot\mathbf{W}_{b/i} + I_z\begin{bmatrix} M_x \\ M_y \\ 0 \end{bmatrix}\right\} \tag{3}$$

Where M_X and M_Y are the normalized (with respect to I_Z) values of constant, body-fixed torque. The differential equation of motion for each body to first order in W_X, W_Y, ε_3, and ε_4 can now be derived:

$$\begin{bmatrix} \dot{W}_x \\ \dot{W}_y \end{bmatrix} = \begin{bmatrix} \dfrac{-\varepsilon_2 W_y \beta}{1-\varepsilon_1} + \dfrac{\varepsilon_3 \beta^2}{1-\varepsilon_1} \\ \dfrac{+\varepsilon_1 W_x \beta}{1-\varepsilon_2} - \dfrac{\varepsilon_4 \beta^2}{1-\varepsilon_2} \end{bmatrix} + \begin{bmatrix} \dfrac{M_x}{1-\varepsilon_1} \\ \dfrac{M_y}{1-\varepsilon_2} \end{bmatrix} \tag{4}$$

As was stated earlier, the principal axis misalignment results in a constant body fixed torque. The applied torques M_X and M_Y include the spring and damper coupling between the two bodies. The kinematic equations for each body are:

$$\begin{aligned} \dot{\theta}_x &= W_x + \beta\,\theta_y \\ \dot{\theta}_y &= W_y - \beta\,\theta_x \end{aligned} \tag{5}$$

Where θ_X is the pitch angle and θ_Y is the yaw angle.

The spring connection in Fig. 9 was considered important because of the accelerations it could induce on the rotors. Originally, this spring connection was at a very low frequency (~ 1 Hz - close to the bandwidth) and an inner actuator was to perform "fine pointing". However, the cryogenic actuators would be a difficult design problem because of constraints on heat, magnetism and geometry. Fortunately, the Lockheed designed PODS-IV supports have increased the stiffness and allowed the elimination of the inner actuators. These raised the resonant frequency to 30 Hz and had more stable temperature behavior. An initial study by Lockheed[7] showed that control can be achieved without the use of the inner actuators because of this stiffening. It is not necessary to consider these high frequency poles in the design, but they are included in the simulation.

Bandwidth Considerations

There are a number of conflicting factors influencing the pointing control system bandwidth. The need to reject the large disturbances around roll (0.0017 Hz) necessitates a significantly higher bandwidth than the roll rate. In addition, the bandwidth must be high enough to validate the assumption of ignoring roll coupling in design. On the other hand, there are many areas that benefit by a lower bandwidth. A low bandwidth would reduce the amount of control used to unnecessarily track the high frequency sensor noise. Since thrust is at such a premium, this is a critical consideration. Additionally, a low bandwidth will minimize interaction with the higher frequency (>30 Hz) structural resonances. As mentioned above, the bandwidth must be lower than the 100 Hz thruster bandwidth, preventing thruster saturation and minimizing the phase lag due to hysteresis.[13] If possible, it

would also be desirable to keep the pointing control bandwidth lower than the 0.64 Hz suspension system bandwidth to minimize the amount of disturbances affecting the gyroscope rotors.

The controller design process is a balancing of these conflicting needs. This process entails drafting candidate designs, using the transfer functions to determine adequate low frequency rejection, and simulations to verify that the rms pointing requirements are met, sufficient thrust is available, and the rms rotor acceleration is within the required bounds. The resulting classical and modern designs are presented below, after a description of the disturbances used in the simulations.

Disturbance Rejection

The primary task is to reject pointing disturbances. These disturbances fall into two categories: low frequency disturbances acting at DC, orbit, and roll frequencies, and high frequency disturbances at and above the bandwidth of the control system. Included in the second category are the "white noise" disturbances affecting a large band of frequencies. Table 2 lists these disturbances, the frequencies at which they act, and their magnitudes.

Table 2

Satellite Disturbances

	Frequency	Magnitude (dyne-cm)
1. Gravity Gradient	roll±2*orbit	600
2. Inertia Misalignment	steady	300
3. Thruster Misalignment	steady	±200
4. Thruster Bias	steady	±800
5. Solar Pressure	orbit, white	40, 4
6. Air Drag	orbit, 0.1 Hz BW	450, 45
7. Thruster Noise	white	50 rms
8. Structural Noise	white	100 rms
9. Thruster Scale Factors	same as drag	±2000

Of the low frequency disturbances, the simplest to predict are gravity gradient and principal axis misalignment. The gravity gradient torque in body axes is about 600 dyne-cm acting at roll±2*orbit frequencies.

As discussed in the dynamic modeling, misalignment of the principal axes of the satellite can be accounted for by considering two small product of inertia terms. This results in a body axis constant disturbance proportional to ε_3 or ε_4. If one allows for two small pitch and yaw rotations (θ_1 and θ_2) of the principal axes away from the geometric body , then the magnitudes of ε_3 and ε_4 are found by the tensor transformation rule to be:

$$\varepsilon_3 = \theta_2 \varepsilon_1 \text{ and } \varepsilon_4 = -\theta_1 \varepsilon_2 \quad (6)$$

Since the principal axis will be aligned with the roll axis to within half a degree, this misalignment results in a constant disturbance of about 300 dyne-cm (assuming a 10% inertia difference). Another constant disturbance results from a thruster bias of about 2 dyne per thruster, creating a torque of ±800 dyne-cm. In addition, there is a 5% thruster misalignment introducing a high frequency pitch/yaw coupling apart from the gyroscopic roll coupling.

Aerodynamic drag will account for the largest disturbances affecting the spacecraft, both in translational control and attitude control. The largest attitude disturbance does not occur from air drag directly but from a coupling with the translational control system.[20] Due to an assumed mismatch of scale factors of the two thrusters used to compensate for translational drag, a couple is produced that, because of the large moment arm, is much larger than the drag torque. This can be calibrated and reduced during the mission.

The aerodynamic drag cannot be accurately estimated but will be bounded. Density variations with the 11 year solar cycle will cause drag variations depending on launch date and time of year. Because GP-B is an inertially referenced spacecraft, the primary drag torque will act at orbit frequency. It is also known that at 650 km the density is not homogeneous. It is estimated[7,19] that the density will randomly vary ±10% on time scales of approximately 10 seconds. Additional variations may be induced by solar flares.

The target launch date of 1994 is at a low of the solar cycle. We estimate an average density at 650 km of 1.0×10^{-12} kg/m^3 and a worst of 1.6×10^{-12} kg/m^3. Using the worst case density of 1.6×10^{-12} kg/m^3, a planform area of 8 m^2 and a drag coefficient of 2.5, the drag force acting on the satellite at roll±orbit frequency is 90 dynes. For a center-of-pressure/center-of-mass separation of 5 cm, the resulting aerodynamic torque is 450 dyne-cm. Allowing for 10% random variations, the high frequency drag torque is 45 dyne-cm with a bandwidth of 0.1 Hz[7].

Assuming that translational control makes up the drag completely, the disturbance due to thruster scale factor mismatch can be calculated. For a drag force of 90 dynes and a 10% mismatch, there is an excess torque of 9 dynes times the moment arm. For a 2 meter moment arm, this disturbance is 1800 dyne-cm varying at roll±orbit frequencies. This is by far the largest disturbance on the satellite. For a translational control system bandwidth of 0.5 Hz, there will be a coupling from the random drag force of 180 dyne-cm at a bandwidth of 0.1 Hz.

Solar pressure disturbances are found in a similar manner to aerodynamic drag. For a solar pressure force[10] of 1 dyne/m^2, an area of 8 m^2, and a 5 cm moment arm, the solar pressure torque is 40 dyne-cm varying at roll. A 10% random variation in solar pressure only produces a 4 dyne-cm torque, small compared to the other random disturbances. Considering again thruster scale factor mismatch a torque is produced of 160 dyne-cm at roll±yearly and a 16 dyne-cm rms white noise torque.

Under the high frequency disturbance category falls thruster noise, structural noise, and micrometeorite impact. Bull[12] estimates thruster noise to be approximately 50 dyne-cm per thruster rms. He also estimates structural noise to be 100 dyne-cm^2/Hz. Structural noise results from a variety of sources, including "thermal expansion and contraction of the outer

satellite, structural stress relief, crinkling of the superinsulation, twitching of the fiberglass supports and dewar plumbing, and vibrations from the telescope chopper wheels."[6] Bull also predicts a 1% probability of micrometeorite encounter during the 1 year experiment, imparting an angular impulse to the satellite of approximately 4 arcsec/sec. This is not considered in these simulations.

Classical and Modern Designs

Reference 7 presents a number of both classical and modern pointing control designs showing that stiffening the satellite obviated the need for inner actuators. This work modified them somewhat after considering more detailed disturbance models and accounting for the gyro suspension system. These designs assumed a rigid body plant ($1/s^2$). The designs are presented in Table 3. Root loci for the classical and modern designs are shown in Figs. 10 and 11.

Table 3

Control System Designs

	Design Plant	Compensator	Simulated Plant	Stability Margins	Comments
Classical	$2 \times \frac{1}{s^2}$	$\frac{4.74 \times 10^5 (s+1)^3 (s+0.5)}{s^2 (s+10)^3 (s+30)}$	Roll Coupled $\frac{1}{s^2}$ 2-Axis Spring	GM = 10.6 dB PM = 60 degrees Crossover = 0.5 Hz	Double Integral Control 6th Order Compensator
Modern	$2 \times \frac{1}{s^2}$	$\frac{1.74 \times 10^3 (s+0.46 \pm 0.38j)}{s (s+5.32 \pm 5.24j)}$	Roll Coupled $\frac{1}{s^2}$ 2-Axis Spring	GM = 13.1 dB PM = 41 degrees Crossover = 0.3 Hz	Single Integral Control 3rd Order Compensator

Note that the classical design includes double integral control to reduce the low frequency disturbances. This is a straightforward way of guaranteeing high open loop gain at low frequency with a low bandwidth control system. In addition, the extra high frequency pole helps roll off the frequency response to reduce the gain near the known resonance.

The modern compensator was designed with single integral control to ensure zero steady state error to the step disturbances. This design was found by computing the LQG full state feedback with high control weighting (1/8000 dyne-cm) and an angle weighting of 1/20 marcsec. The regulator roots are the low frequency roots clustered near the origin in Fig. 11. An LQG estimator was designed for 1 marcsec^2/Hz sensor noise and 250,000 dyne-cm^2/Hz process noise (see below), accounting for the high frequency roots in Fig. 11. Because of concern that the single integrator would not provide enough low frequency gain, a notch was originally added at roll frequency. However, it was found through simulation that this was unnecessary to meet the requirements, required more control authority, and merely added complexity.

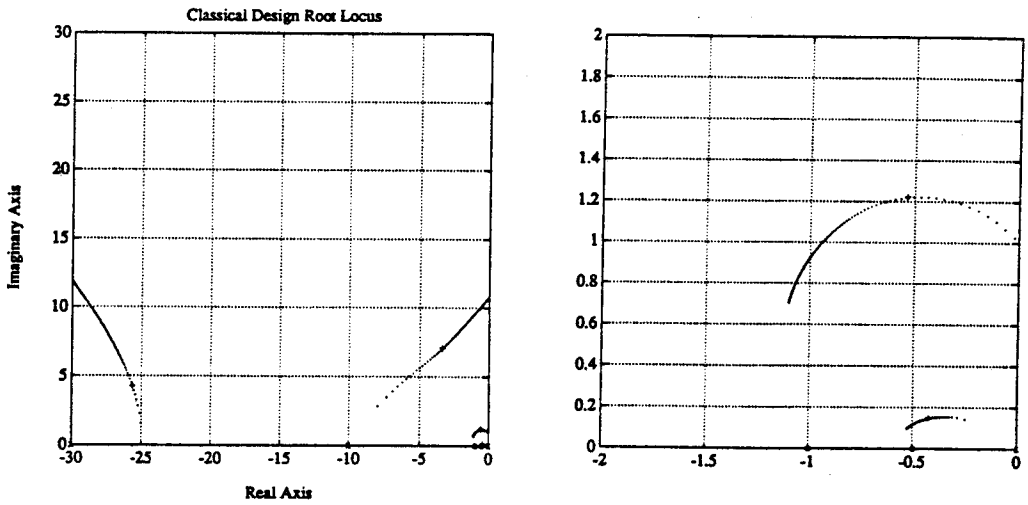

x = open loop poles, o = open loop zeros, + = closed loop roots

Figure 10: Classical Compensator Root Loci

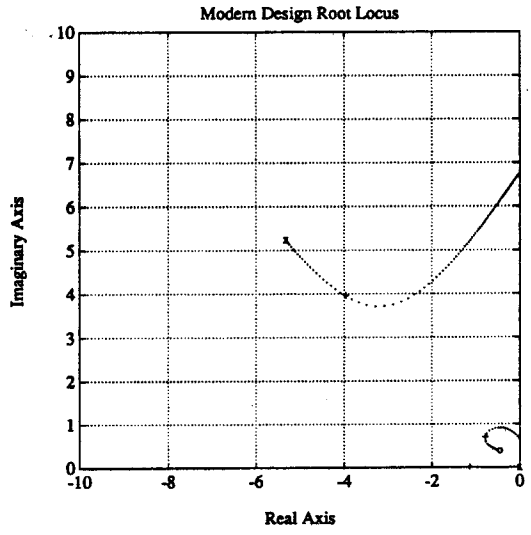

x = open loop poles, o = open loop zeros, + = closed loop roots

Figure 11: Modern Compensator Root Locus

SIMULATION RESULTS

Simulations were performed for each of the above compensators to verify that all of the specifications were met. Because only linear system models were considered, superposition held and each of the important effects - low frequency disturbances, disturbance noise, and sensor noise - could be simulated separately and the results added. Closed loop transfer functions were found from disturbances to pitch and yaw angles and rotor accelerations. These were converted to state space form, discretized, and simulated using the Pro-Matlab™ computer package. The standard discrete form of these equations is:

$$x_{n+1} = \Phi(\Delta t)x_n + \Gamma u + w \tag{9}$$

Here, Δt is the step size, Φ is the state transition matrix, u is the deterministic input, and w is the random input. The covariance of w for the stochastic simulations was found by numerically solving the covariance integral:

$$W = \int_0^{\Delta t} \Phi(\tau) Q \Phi^T(\tau) d\tau \tag{10}$$

where Q is the spectral density of the continuous white noise disturbances and W is the covariance matrix of the discrete process noise, w.

The simulations included all of the above low frequency disturbances as u, that is, gravity gradient, principal axis misalignment, thruster misalignment of 5%, thruster bias of 2 dynes/thruster, air drag, and 10% thruster scale factor mismatch. The white disturbance noise was chosen to have a spectral density of 500 dyne-cm/$Hz^{1/2}$. Though this is high compared to the values quoted in Table 2, it is felt that by being very conservative with the process noise spectral density we are both assuring the validity of the response to the present disturbance models and bounding the ability of the control system. The response was also found for sensor noise having a spectral density of 1 marcsec/$Hz^{1/2}$.

Steady State Response

The simulation results for both designs are listed in Table 4. Plots of the results integrated over one-half an orbit (the length of one data taking phase before occultation) are presented in Figs. 12 to 17. Both the classical and modern controllers satisfied all of the low frequency requirements, keeping pitch and yaw angles within 0.04 marcsec for the classical design and 2.5 marcsec for the modern. Note that both have zero steady state error but non-zero control torque due to the constant disturbances. Also observe that because it only has single integral control, the modern controller allows larger excursions. The difference in control authority used is not noticeable. It is also interesting to note that the rotor accelerations for the classical design are an order of magnitude below that of the modern design. Both designs, however, have accelerations within the $1x10^{-10}$g limit stated by Keiser.[17] The control torque is below 3000 dyne-cm maximum for both designs, with a constant bias of approximately 600 dyne-cm.

Table 4

Simulation Results
Maximum Responses To Disurbances and Telescope Noise

	Pointing Error (marcsec) req. ≤ 70	Control Torque (dyne-cm) req. ≤ 10,000	Gyro Acceleration (nanog) req. ≤ 800
Telescope Noise	6 classical	400 classical	30 classical
	6 modern	300 modern	10 modern
Disturbance Noise	30 classical	3000 classical	40 classical
	50 modern	2000 modern	50 modern
Low Frequency Disturbances	0.04 classical	3000 classical	0.0007 classical
	3 modern	3000 modern	0.0009 modern
Absolute Sum	36 classical	6400 classical	70 classical
	59 modern	5300 modern	60 modern

Because of its higher gain at low frequency and faster rolloff at high frequency, the classical design outperformed the modern one in response to disturbance noise. While the modern controller had an rms response to disturbances of approximately 20 marcsec, the classical one had an rms response of about 10 marcsec. On the other hand, the classical controller used about 1000 dyne-cm more of control authority. In both cases, the rotor acceleration was about 10 nanog rms, more than an order of magnitude below the limit set by Keiser.

Both controllers responded about the same to sensor noise. Note that these plots are of real attitude response to sensor noise; they are not corrupted by the sensor noise. Both designs used about 100 dyne-cm of thrust on average and again had a mean square rotor acceleration below 10 nanog.

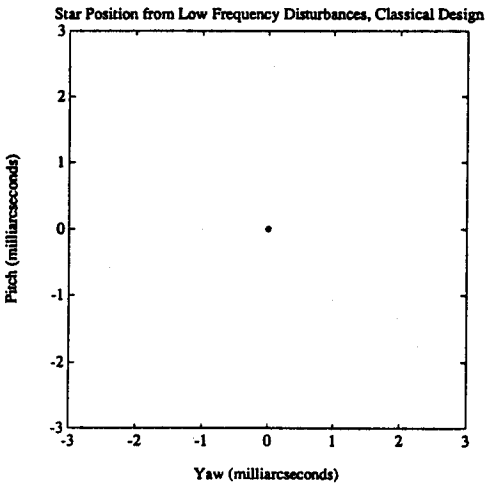

(a)
Required Postion ≤ 70 marcsec

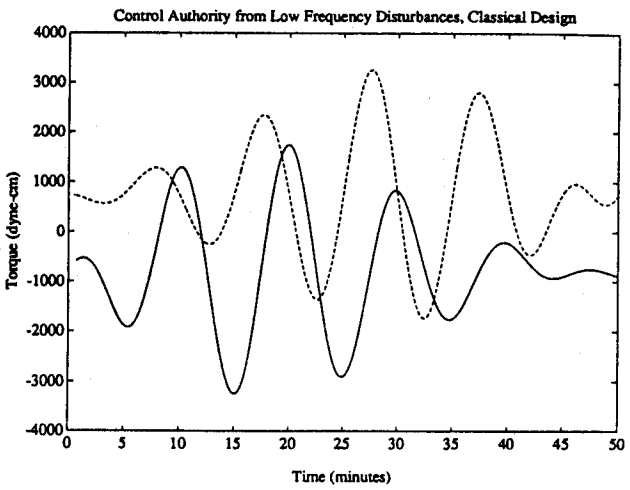

(b)
Required Torque ≤ 10,000 dyne-cm

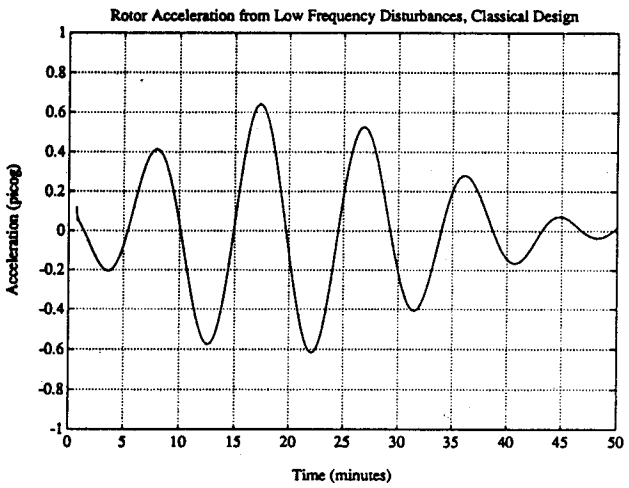

(c)
Required Acceleration ≤ 100 picog

Figure 12: Classical Design Responses to Low Frequency Disturbances

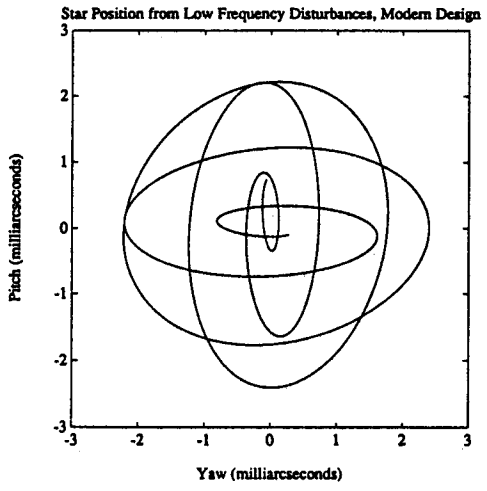

(a)
Required Postion ≤ 70 marcsec

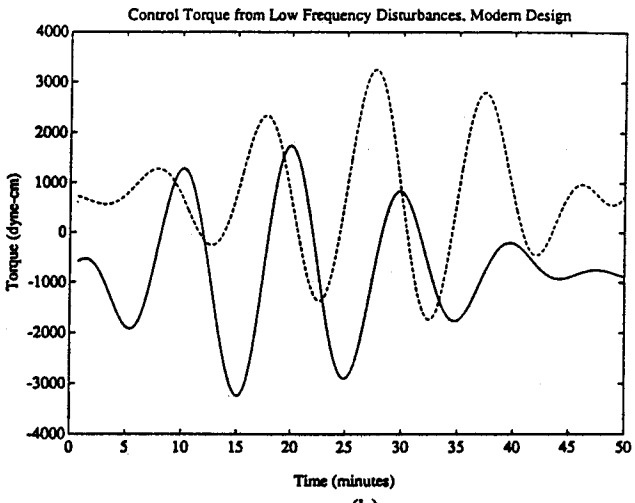

(b)
Required Torque ≤ 10,000 dyne-cm

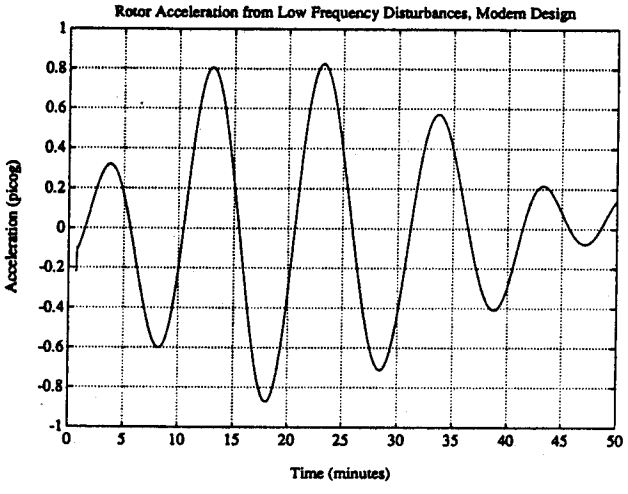

(c)
Required Acceleration ≤ 100 picog

Figure 13: Modern Design Responses to Low Frequency Disturbances

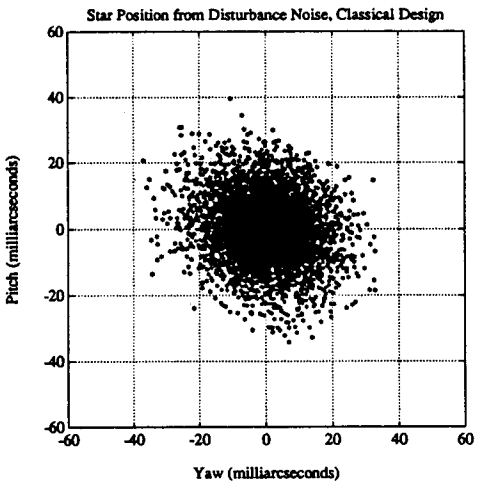

(a)
Required Postion ≤ 70 marcsec

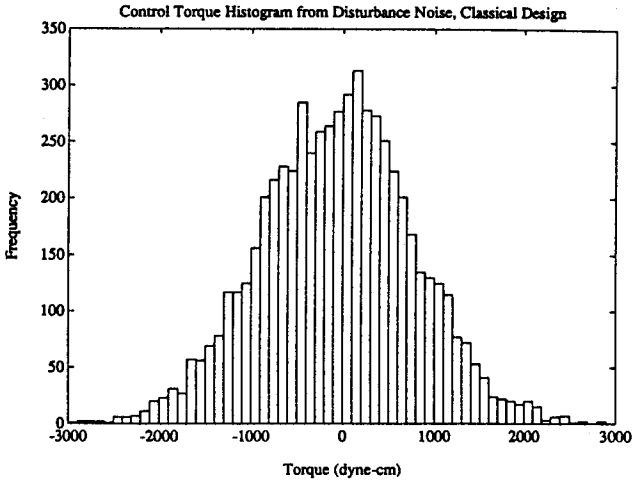

(b)
Required Torque ≤ 10,000 dyne-cm

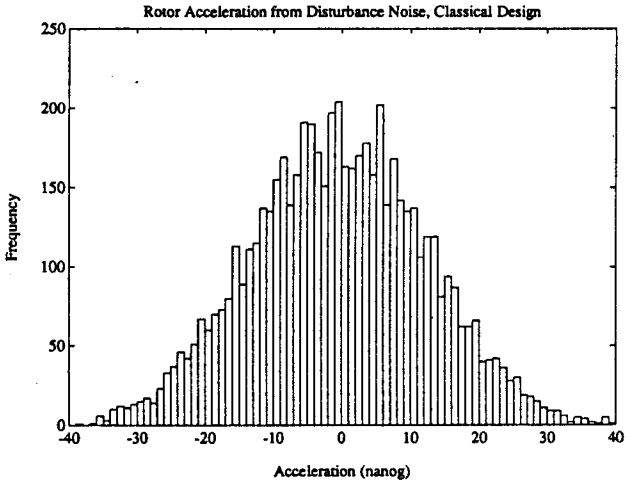

(c)
Required Acceleration ≤ 200 nanog rms

Figure 14: Classical Design Responses to Disturbance Noise

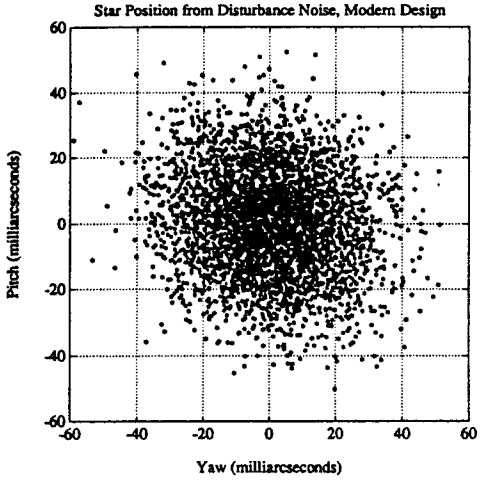

(a)
Required Postion ≤ 70 marcsec

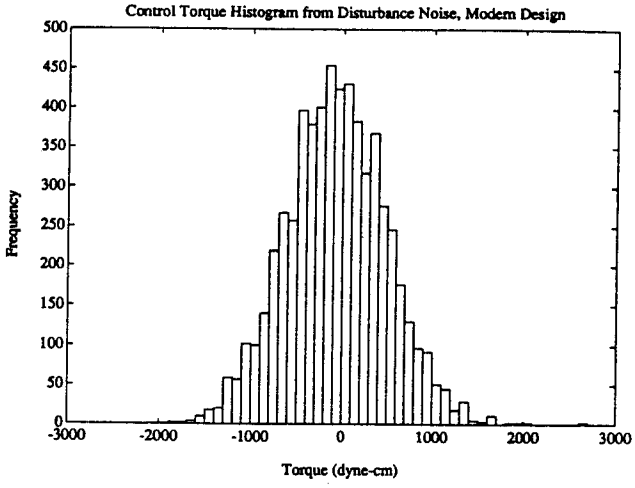

(b)
Required Torque ≤ 10,000 dyne-cm

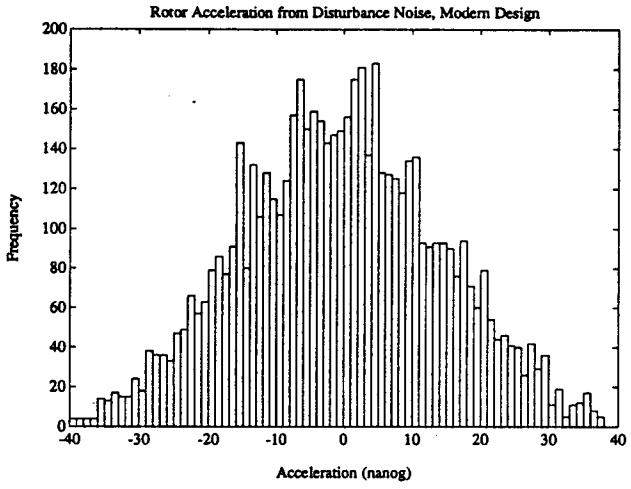

(c)
Required Acceleration ≤ 200 nanog rms

Figure 15: Modern Design Responses to Disturbance Noise

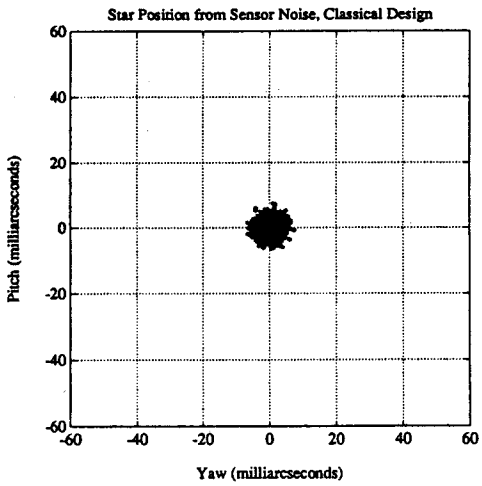

(a)
Required Postion ≤ 70 marcsec

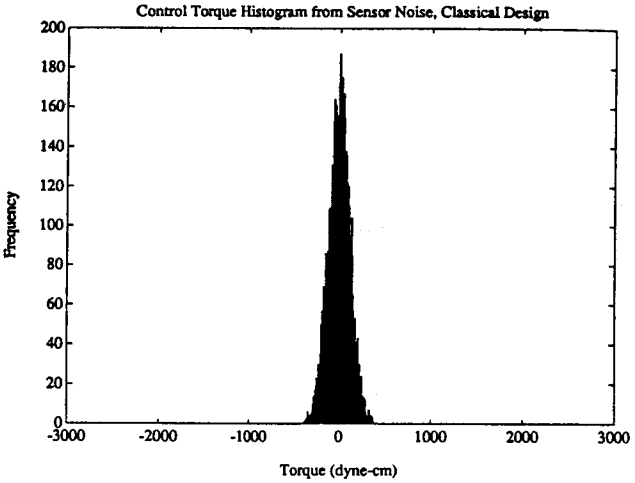

(b)
Required Torque ≤ 10,000 dyne-cm

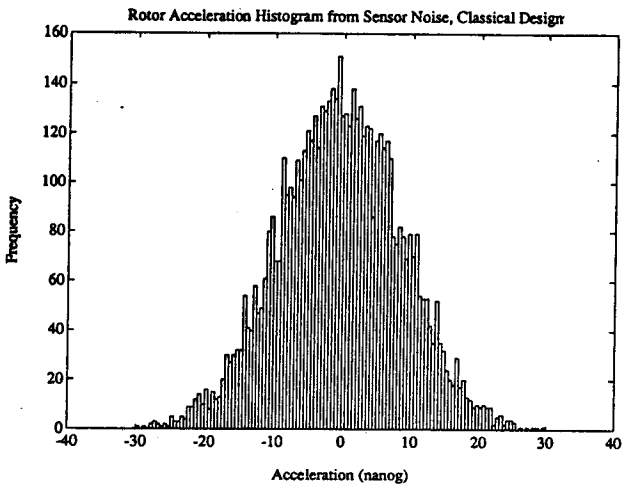

(c)
Required Acceleration ≤ 200 nanog rms

Figure 16: Classical Design Responses to Sensor Noise

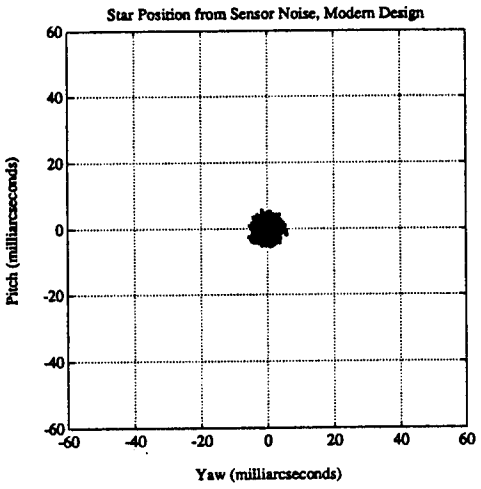

(a)
Required Postion ≤ 70 marcsec

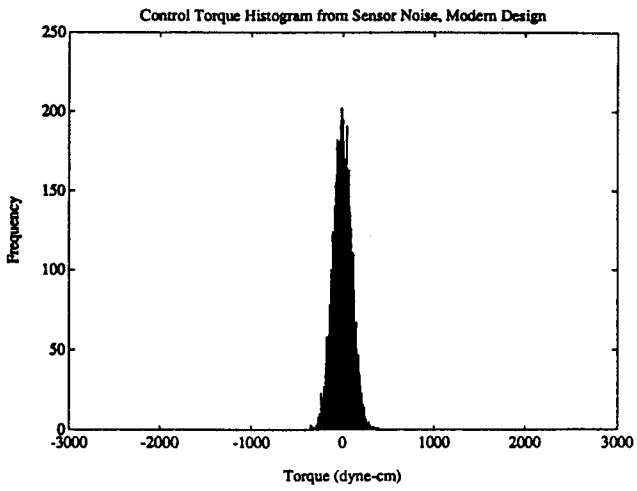

(b)
Required Torque ≤ 10,000 dyne-cm

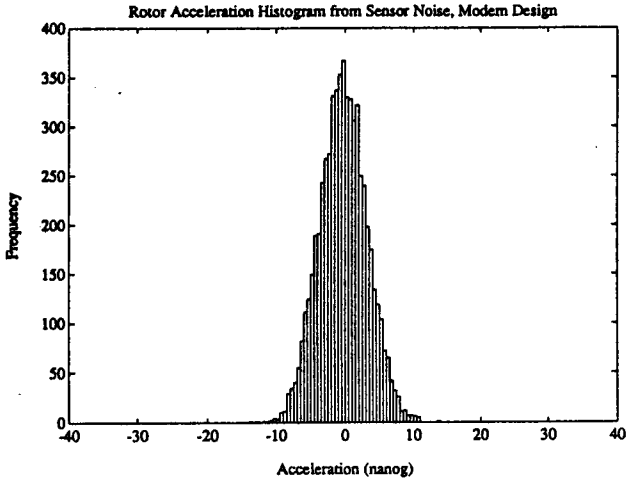

(c)
Required Acceleration ≤ 200 nanog rms

Figure 17: Modern Design Responses to Sensor Noise

CONCLUSION

This paper has presented all of the major requirements and constraints on the pointing control system. Two controller designs were considered and while both met the specifications, the following conclusions were reached:

1. The modern design is preferred because of its simplicity.

2. The modern design achieved a pointing accuracy $\leq$ 60 marcsec against a requirement of 70 marcsec.

3. The maximum torque demand is only 53% of the design capacity which assumes only one-half of the thrusters are available.

4. The root mean square induced accelerations on the gyros are $\leq$ 20 nanog which is 10% of the maximum allowable accelerations of 200 nanog.

Because of the unique star-sensor and proportional helium thrusters, we were able to synthesize a design that met all of the critical requirements of the GP-B attitude control system within a significant margin of safety. Although, as mentioned, there are a number of additional issues being investigated, we do not believe they adversely affect the design. This control accuracy will allow for the most precise measurement of Einstein's General Theory of Relativity ever attempted.

REFERENCES

1. Parkinson, Bradford W., C.W. Francis Everitt, and Daniel DeBra. The Stanford Relativity Gyro Experiment. reprinted from *Guidance and Control,* Vol. 63, *Advances in the Astronautical Sciences,* AAS, etc.
2. Parkinson, B.W., C.W.F. Everitt, J.P. Turneaure, and R.T. Parmley. The Prototype Design of the Stanford Relativity Gyro Experiment. *38th Congress of the International Astronautical Federation,* October 10-17, 1987/Brighton, United Kingdom. IAF-87-458.
3. Everitt, C.W.F. Preface, Papers on the Stanford Relativity Gyroscope Experiment. Reprints from *Proceedings of SPIE - The International Society for Optical Engineering*. Vol. 619, 23-24 January, 1986.
4. Bardas, D., et.al., Hardware Development for Gravity Probe -B. Ibid.
5. Young, Lou S. Systems Engineering for the Gravity Probe-B Program. Ibid.
6. Fairbank, W.M, C.W.F. Everitt, D.B. DeBra, et. al. Report on a Program to Develop a Gyro Test of General Relativity in a Satellite and Associated Control Technology. June, 1980.
7. Breakwell, J.A., E.K. Parsons, D.B. Schaechter, and R.H. Vassar. Inner-Actuator Trade Study for Gravity Prob B Pointing Control System. 30 August 1985. Unpublished report.
8. Van Patten, Richard A. Flight Suspension for the Relativity Gyro. in Hu Ning (ed.), *Proceedings of the Third Marcel Grossman Meeting on General Relativity.* (Science Press and North-Holland, 1983).
9. Lockhart, James M. SQUID Readout and Ultra-low Magnetic Fields for Gravity Probe-B (GP-B), Papers on the Stanford Relativity Gyroscope Experiment. Reprints from *Proceedings of SPIE - The International Society for Optical Engineering*. Vol. 619, 23-24 January, 1986.
10. Parmley, R.T., J. Goodman, M. Regelbrugge, and S. Yuan. Gravity Probe B Dewar/Probe Concept. Ibid.
11. Everitt, C.W.F., D.E. Davidson, and R.A. Van Patten. Cryogenic Star-Tracking Telescope for Gravity Probe B. Ibid.
12. Bull, John S. Precise Attitude Control of the Stanford Relativity Staellite. March 1973, Stanford Ph.D. Thesis.
13. Chen, Jeng-Heng. Helium Thruster Propulsion System for Precise Attitude Control and Drag Compensation of the Gravity Probe-B Satellite. December 1983. Stanford Ph.D. Thesis.
14. Lorell, Kenneth R. and Benjamin Lange. Precision Attitude Control of Symmetric Spinning Bodies. April 1971. Stanford Ph.D. Thesis.
15. Iufer, E.J. Cryoperm Shield Performance Test. Preliminary. Unpublished report of September 17-18, 1987.
16. Cabrerra, Blas. Torques on Mu-metal Shields from Earth's Field. 27 August, 1985. Unpublished Report.
17. Keiser, G.M. Suspension Torques on a Gimballed Electrostatically Supported Gyroscope and etc. Feb., 1985. Unpublished Report.
18. Parkinson, Bradford W. Closed-Form solution for Motion of a Spining Rigid Body. *Journal of Spacecraft and Rockets*. July 25, 1967.
19. DeBra, D.B.. Private Conversation.
20. Wichtor, Peter. Coupling Between Translation and Pointing Control in the GP-B Spacecraft. 15 December 1987. Unpublished Report.